UNIVERSIDADE DE SÃO PAULO

PUBLICAÇÕES

DYNAMICS OF THE TWO-FREQUENCY TORUS BREAKDOWN IN THE DRIVEN DOUBLE SCROLL CIRCUIT

M.S. Baptista, I.L. Caldas
Instituto de Física, Universidade de São Paulo

Pag. 1 - 20

Dynamics of the two-frequency torus breakdown in the driven Double Scroll circuit

M. S. Baptista, I. L. Caldas

Institute of Physics, University of São Paulo

C. P. 66318, CEP 05315-970 São Paulo, S.P., Brazil

Abstract

In this work we numerically identified three scenarios for the two-frequency torus breakdown to chaos, in the driven Double Scroll circuit, for varying driven parameters. Two of these scenarios follow the Curry-Yorke route to chaos. For one scenario, we identified the transition to chaos through the onset of a heteroclinic tangle and its heteroclinic points. In the other scenario, chaos appears via period-doubling bifurcations. The third scenario is through the type-II intermittency for wich a quasiperiodic torus grows in size, and breaks by touching external saddle points, forming a heteroclinic saddle connection. These identified dynamic scenarios have distinct structure evolutions. Thus, for the Curry-Yorke route, chaos appears softly and alternates with phase-locking, while, through type-II intermittency, chaos appears abruptlly and is preserved for a large range of the varying driven parameter.

I. INTRODUCTION

In this paper we report the dynamical scenarios for the route to chaos found numerically for a driven electronic circuit. Our investigation was motiveted by the relevance of the observed two-frequency torus breakdown to the general dynamical systems theory.

The routes to chaos, found in nonlinear systems by varying control parameters, are important because they are used to predict the transition from a regular oscillation to a irregular one [1], [2].

One well known example of route to chaos is the infinite sequence of period-doubling bifurcations [3], [4], universal for a large class of one varying parameter systems.

Another possible route is the destabilization of the three-frequency torus [5]. This route has a dynamical scenario through which chaos can appear just after the third Hopf bifurcation, in other words, after the appearance of a third frequency into the system [6] and [7]. In this case, an arbitrary small perturbation can lead to the destabilization of a three-frequency oscillation. However, for other scenarios, a three frequency quasiperiodic movement can also persist under a large perturbation [8], [9], and [10]. Indeed, chaos is more common to appear as higher is the number of frequencies [9].

Moreover, chaos can also occur directly through a destabilization of a two-frequency torus as proposed by Curry and Yorke [11], [12]. This general route happens through different scenarios leading to typical folds and wrinkles in the broken torus.

Thus, in this last route, chaos can appear, for two-parameter families of maps of the plane, through the destabilization of a two-frequency phase-locked trajectory [13], [14]. After chaos appears, topological alterations are responsible for the loss of the smoothness of the two-frequency torus.

In the same route, chaos also emerges from two-frequency torus through the period-doubling scenario [15]. In this case, a phase-locked band chaos comes into sight with a rational rotation number.

However, most of the previous works, about the two-frequency torus breakdown, does not address the topological transitions induced by the driving parameters, difficult to recognize in dissipative systems, since the homo and heteroclinic tangles contract along the stable direction. Nevertheless, Refs. [13] and [14] contain an overview of the possible topological transitions for the two-frequency torus breakdown to chaos.

In this paper we deal with the Matsumoto's electronic circuit [16] (also known as Chua's circuit) perturbed sinusoidally. This is a simple nonlinear circuit with a piecewise-linear resistor that has been studied because of its electronic simplicity and variety of non-linear phenomena. The driven versions of this circuit have been extensivelly investigated and many bifurcation phenomena (not observed in the non perturbed circuit) have been found [17],

[18], [19], [20], [21], [22] [23].

The onset of chaos by torus breakdown in the Matsumoto's circuit, describing a chaotic attractor known as Double Scroll [24]), and driven by a sinusoidally perturbation, is investigated in Refs. [17] and [20]. In this case, this circuit is known as driven Double Scroll circuit. However, no topological or dynamical analysis is presented and untill now the scenarios for the appearance of chaos by torus breakdown in the driven Double Scroll circuit remains unknown.

In this paper we show that chaos appears by the Curry-Yorke route through period-doubling or phase-locking scenarios. We show that chaos preceeded by phase-locking is due to the transversally crossing of the strong stable foliations with the stable manifolds of the knots in the phase-locked trajectory.

In addition, we found that chaos, in the considered driven circuit, can also appear through type-II intermittence [21]. In the present paper, a dynamical scenario for this destabilization is proposed. So, in this case, the two-frequency quasiperiodic torus looses its stability by touching external saddle points that form a heteroclinic saddle connection. This nonlinear mechanism [25] is responsible for the reinjection necessary for the existence of type-II intermitence.

In summary, in the driven Double Scroll circuit, chaos appears in two observable ways, characterized by distinct Lyapunov exponent evolutions and topological changes as a driving parameter is varied. Namely, for the Curry-Yorke route, these transitions occurs softly in contrast with the hard transitions associated to type-II intermittency.

In Sec. II we present the driven Double Scroll circuit. In Sec. III we analyse dynamically the Curry-Yorke route to the onset of chaos in this circuit. In Sec. IV we present the new scenario for which chaos appears, in the same circuit, through a type-II intermittence and, finally, conclusions are given in Sec. V.

II. The driven Double Scroll circuit

The Double Scroll circuit [16] is shown in Fig. 1 with its three energetic components: two capacitors, C_1 and C_2, and one inductor, L. It has also two resistors, R and r, and the non-linear resistor, R_{NL}, whose characteristic
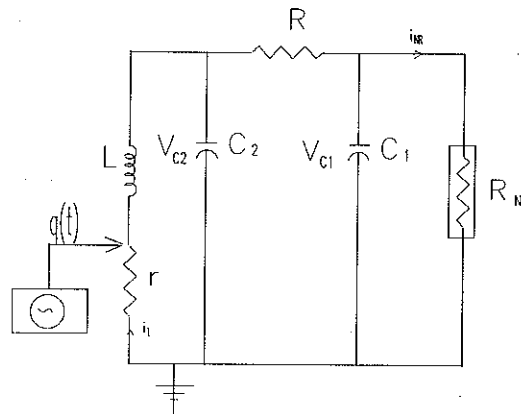
curve can be seen in Fig. 2.

Figure 1: The Double Scroll circuit. The electronic value components used in this paper are: $C_1 = 0.0052\mu F$, $C_2 = 0.056\mu F$, $R = 1470\Omega$, $L = 9.2mH$, and $r = 10\Omega$.

The R_{NL} characteristic curve is mathematically represented by

$$i_{NR}(V_{c1}) = m_0 V_{c1} + 0.5(m_1 - m_0) \mid V_{c1} + B_p \mid + 0.5(m_0 - m_1) \mid V_{c1} - B_p \mid \quad (1)$$

The driving force applied across the resistor r is represented by

$$q(t) = V \sin(2\pi f t) \quad (2)$$

where V is the amplitude and f is the frequency.

We can simulate the circuit of Fig. 1 by applying Kirchoff's laws. So, the resulting state equations are

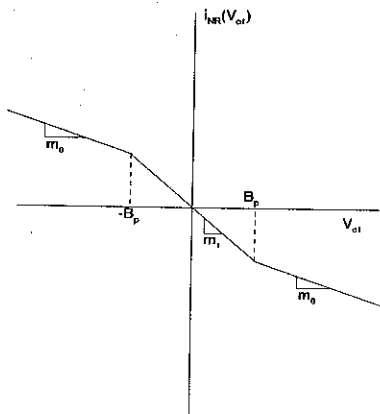$$C_1 \frac{dV_{C1}}{dt} = \frac{1}{R}(V_{C2} - V_{C1}) - i_{NR}(V_{c1})$$

3

4

Figure 2: The characteristic curve of the non-linear resistor R_{NL} where B_p=1.0, m_0=-0.5, and m_1=-0.8.

$$C_2 \frac{dV_{C2}}{dt} = \frac{1}{R}(V_{C1} - V_{C2}) + i_L \qquad (3)$$

$$L \frac{di_L}{dt} = -V_{C2} - q(t)$$

where V_{C1} and V_{C2} are the voltage across the capacitors C_1 and C_2, respectively, and i_L is the electric current across the inductor L.

To avoid numerical problems we used a rescaled set of parameters given in terms of the real values (given in Fig. 1). Thus, the parameters used in Eqs. (3) for doing numerical simulation of the circuit in Fig. 1 were $\frac{1}{C_1} = 10.0$, $\frac{1}{C_2} = 1.0$, $\frac{1}{L} = 6.0$, $\frac{1}{R} = 0.6$ the initial conditions were $V_{c1}(0) = 0.15264$, $V_{c2} = -0.02281$, $i_L(0) = 0.38127$, and the step size was $dt = 0.005$. For integrating Eqs. (3) we used the fourth-order Runge-Kutta algorithm.

For these parameter simulation values, and null perturbing amplitude, $V = 0$, the circuit behaves chaotically. As the circuit is dissipative its dynamic variables (V_{C1}, V_{C2}, and i_L) evolve on a chaotic attractor named Double Scroll [16].

One of the most known tools for measuring chaos is the Lyapunov spectrum formed, in this case, by three Lyapunov exponents λ_n. Thus, for the considered system, depending on the nature of (λ_1, λ_2, λ_3), we can char-

acterize an oscillation as follows: $(+, 0, -)$ a chaotic attractor; $(0, 0, -)$ a quasi-periodic moviment on a torus T^2; $(0, -, -)$ a limit cycle; $(-, -, -)$ a fixed point. Although we computed the three Lyapunov exponents, in this work we show only the first one. That is because we are mainly interested in determining how chaotic is the system.

In this paper, we calculated the Lyapunov exponents by applying the Eckmann-Ruelle algorithm [12], [26], with a transient $n = 100$, and a time step $dt = 0.005$ during an integration time $t = 3882$ which corresponds to $n \approx 700$. The Gram-Schmidt orthonormalization was applied each 10 steps.

Due to the non exact computation of these exponents, we considered the first Lyapunov exponent positive if $\lambda_1 \gtrsim 0.005$, within the used numerical precision.

All results shown in this paper were due to numerical simulations. Complementary information about the considered experiments are given in Ref. [21].

III. Soft appearance of chaotic motion

A dynamical overview of the Curry-Yorke route can be seen (for a rising frequency, f, and a fixed amplitude, V) in the bifurcation diagram of Fig. 3A and by analysing the first Lyapunov exponent of Fig. 3B. These figures show phase-locking of quasiperiodic tori, onset of chaos, and further phase-locking alternating with chaotic motion. For the considered parameters, the Lyapunov exponent increases slowly with f. For f close to 0.1978, the exponent reaches a value $\lambda \gtrsim 0.05$ and after that phase-locking is not anymore observed.

The four regions indicated in Fig. 3A, denoted by A_1, A_2, A_3, and A_4, have their correspondent attractors shown on the Poincaré sections of Fig. 4. So, Fig. 4A shows the quasiperiodic attractor indicated by A_1 in Fig. 3A. Figure 4B shows the period-17, phase-locked attractor, indicated by A_2 in Fig. 3A. Finally, Figs. 4C and 4D show the chaotic attractor indicated by A_3 and A_4.

As we see in Fig. 3A, after the onset of chaos, the first Lyapunov exponent increases slowly with f. Additionally, the chaotic trajectory obtained in the Curry-Yorke scenario is confined to the region previously occupied by the previous stable quasi-periodic torus. Only for higher values of f the

trajectory escapes the toroidal surface neighborhood. Because of these characteristics, we refer to this transition as a soft onset of chaos.
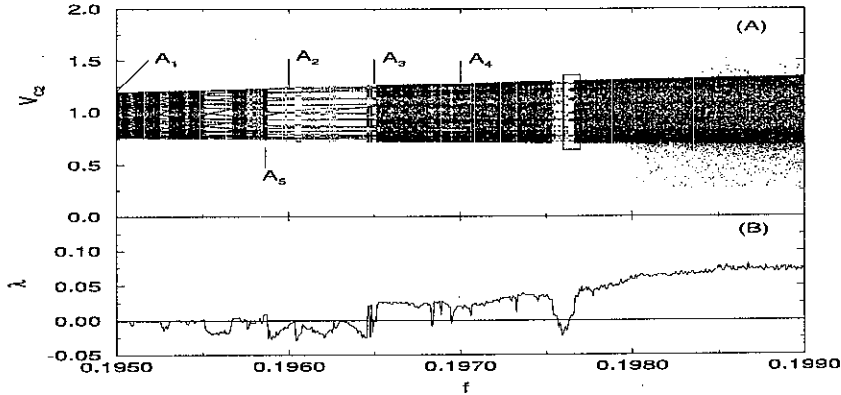

Figure 3: (A) A bifurcation diagram for a rising amplitude f and a fixed driving amplitude $V = 0.20$, showing that phase-locked regions come into sight within quasi-periodic regimes and also in the chaotic regimes. So we indicated five regions we will focus our analysis. In A_1 we have a quasi-periodic attractor, A_2 a period-17 phase-locked attractor which coexist with other period-N attractors, A_3 and A_4 we have the onset of chaos through phase-locking, and A_5 one of the regions where we find weak chaos. (B) The first Lyapunov exponent λ, for the same parameters of (A). That means chaos for $\lambda > 0$. $V_{C1} = -1.5$.

In Fig. 4C we see that the smooth and closed quasi-periodic attractor (in Fig. 4A), after phase-locking (4B) and the onset of chaos, becomes a folded and rough attractor. Further amplifications of these folds would reveal a fractal structure and also the streching and folding characteristics of chaotic regimes. So, in this case, chaos can be better recognised by analysing the geometric structure of the attractor than by computing the Lyapunov exponent. Consequently, this procedure could be considered when the first Lyapunov coeficient values can not be distinguished from zero.

However, in the case of Fig. 4D, a small amplification already reveals the mentioned geometric properties. This figure shows also a phase-unloked, nine-band, chaotic attractor. The evolution of the region n is given by the region $n + 1$. Thus, we clearly see that region 2 is the region 1 folded along a
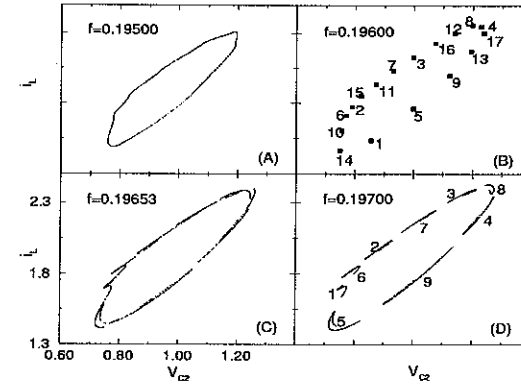

Figure 4: (A) Quasiperiodic two-frequency torus (region A_1 in Fig. 3), (B) Period-17 phase-locking (region A_2), a chaotic attractor with many folds (region A_3), and a nine-band chaotic attractor (region A_4). $V_{C1} = -1.5$.

direction transversal to the torus and streched along a direction tangent to the torus surface.

The observed folding and streching processes and the computed Lyapunov exponent assure us that the trajectory is chaotic. However, we want to see how is the transition from a phase-locked trajectory to the chaotic one. For this purpose we analysed the attractor when (for the used numerical precision) we first observed the onset of chaos. So, in Fig. 5 we see a toroidal-shaped attractor, which is actually chaotic. This attractor for a very small change on the value of the driving frequency becomes a period-17 phase-locked orbit. Although the Lyapunov exponent is positive, its value is very small. Thus, in this example, chaos should not be characterized by analysing only this exponent. So, a geometric interpretation of this toroidal-shaped attractor must also be considered for characterizing the transition to chaos.

Before the onset of chaos shown in Fig. 5, the only attractor observed was the period-17 phase-locked one. To examine the influence of this attractor on this transition, we examine in Fig. 6 the amplification of the box in Fig. 5, particularly the geometry nearby the unstable period-17 attractor.
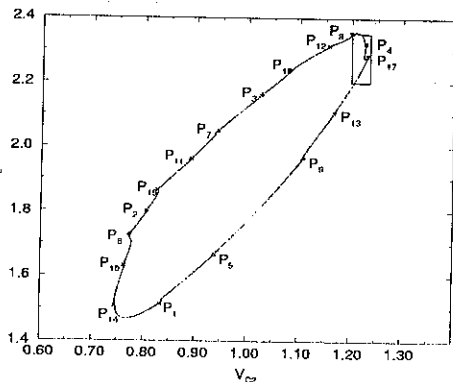
7

8

Figure 5: Poincaré section of the chaotic attractor for f indicated by A_5 in Fig. 3.

To guide that, let us introduce a mapping G that models the trajectory in the Poincaré section of Fig. 5. If we consider each period-17 unstable point represented by P_n (with $n = 1, \ldots, 17$), then, $G^{17}(P_n) = P_n$, and $G(P_n) = P_{n+1}$. In addition, $G^{17}(P_n + \epsilon)$ leaves this point to the nearest point in the clockwise direction. Thus, for example, $G^{17}(P_4 + \epsilon)$ approaches P_{17}.

To identify the chaotic characteristics of the trajectory shown in Fig. 5, we plot in Fig. 6 the region around the points P_4 and P_{17}. The points in the large gray region denoted by X_0, when iterated by $G^{17}(X_0)$, rest in the large black region denoted by X_{17}. The small box in this region is magnified and we see that the region X_{17} is in fact composed by two regions. The region X_0 under the mapping G suffers a streching along the unstable manifold, W^u, tangent to the torus, and a fold along the stable direction, W^s (corresponding to the strong stable foliation), transversal to the torus at the point P_{17}. In fact, these manifolds are neither exactly transversal nor tangent to the torus surface, since the mapping near the fixed points is exact and not a linearized one. The same points iterated by $G^{34}(X_0)$, spread along the unstable direction and squeezed along the stable one, due to the dissipative effects. So, this and further iterations are difficult to show.

A point somewhere in X_0 takes a positive infinite time to reach the point P_{17} along W^s, and a negative infinite time to reach P^{17} along W^u. As the
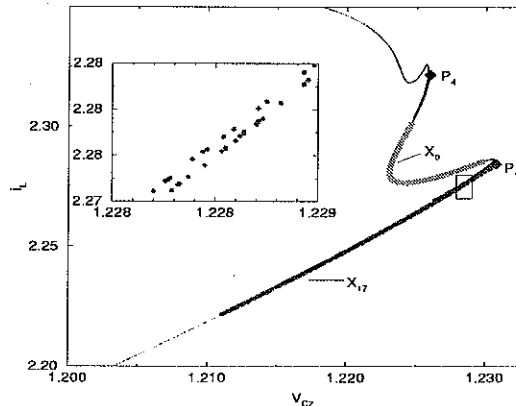

Figure 6: Magnification of Fig. 5 showing a region (large gray line) X_0 that after 17 Poincaré section crossings is transformed into the region X_{17}. So X_0 streches along the unstable manifold of the point P_{17} and folds along the stable manifold of this point. Within the box we see a magnification of the region X_{17}.

unstable manifold of the point P_{17} drives the trajectory to other saddle point, the point P_{17} is a heteroclinic point.

So, in this case, for a varying driven parameter, chaos actually appears from a period-17 phase-locked trajectory that is seen in the Poincaré section as seventeen knots. Between each two of these knots, there is one saddle point. The unstable manifolds of these saddle points direct the trajectory toward these knots. The scenario from the onset of chaos is the following: the unstable manifold of the saddle points crosses transversaly the strong stable foliation (due to the repellor focus). The existence of this scenario was theoretically predicted in [13].

In conclusion, infinite period trajectory, chaos, appears from a finite period, phase-locked one.

Furthermore, chaos can also appears through an infinite sequence of period-doubling bifurcations as seen in Fig. 7. After that, chaotic bands appear with very low Lyapunov coeficients, and may phase-locking. Moreover, the Lyapunov exponent increases its value when the bands merge in only one chaotic band. In Fig. 7 we also see the coexistence of two attrac-
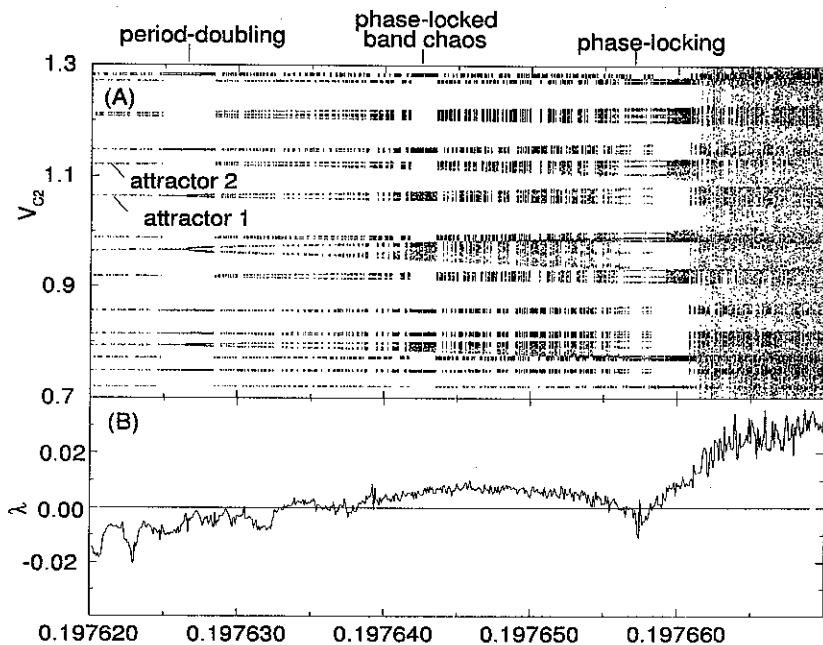
Figure 7: (A) Bifurcation diagram showing coexistence of attractors and the onset of chaos through period-doubling, by a rising driving frequency f and a fixed driving amplitude $V = 0.20$. (B) The first Lyapunov exponent λ, for the same parameters of (A). $V_{C1} = -1.5$.

tors [23], indicated by attractors 1 and 2.

The spectral analysis of the soft onset of chaos is shown in Fig. 8. Figure (A) shows the spectrum for the Double Scroll circuit ($V = 0$). We see two main peaks, one corresponding to the characteristic frequency $f_c \approx 0.29$ [23] and the other, indicated by f_1, corresponding to the frequency with which the trajectory jumps between the two rolls presented in the Double Scroll attractor [16]. For $f = 0.18500$ and $V = 0.20$, in (B), the peaks at f_1 and f_c are destroyed and a peak f corresponding to the driving frequency appears (the way they are destroyed can be seen in Ref. [23]). Increasing frequency
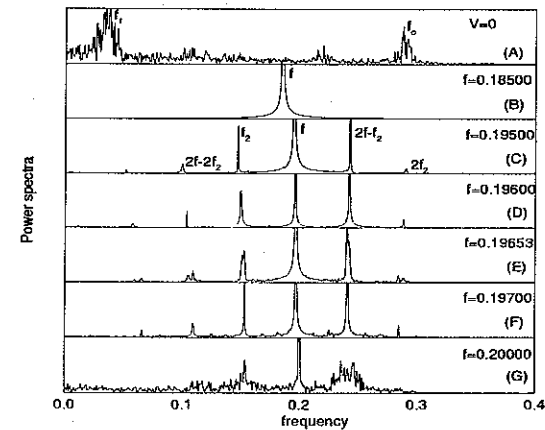

Figure 8: Power spectra of the time evolution of the variable V_{C1}. Spectra of the nonperturbed circuit (A) and for driven varying frequency and fixed amplitude $V = 0.20$; phase-locking in (B), quasi-period oscillation in (C), phase-locking (D), and chaos in (E,F,G).

to $f = 0.19500$ another incommensurable frequency f_2 appears and thus we have a quasiperiodic moviment. In (D) the frequencies f and f_2 become commensurable and so phase-locking occurs. A low amplitude broad band appears in (E) revealing a chaotic attractor, also observed in (F) and (G). Note that Figs. 7C-F correspond respectivelly to Figs. 4A-D.

IV. Abrupt appearance of chaotic motion

The abrupt appearance of chaos, via two-frequency torus breakdown, was investigated through numerical integration of Eqs. (3), for a fixed driving amplitude, $V = 0.28$. Thus, Fig. 9A shows a bifurcation diagram of the variable V_{C2}, when the trajectory crosses a Poincaré section at $V_{C1} = -1.5$, as a function of the driving frequency, f. The abrupt appearance of chaos, seen in this figure, is confirmed by the first Lyapunov exponent, λ (Fig. 9B). Chaos first appears for $f = 0.16897$ leading to $\lambda > 0$.

In this bifurcation diagram, there are no periodic orbits after the onset of chaos. In addition, the first Lyapunov exponent has a large value at the onset of chaos, which is preserved by increasing the frequency f.
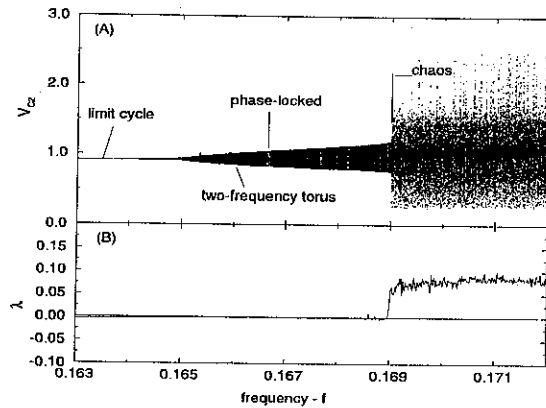
Figure 9: (A) Bifurcation diagram showing the two-frequency torus creation (via Hopf bifurcation) and its destruction, generating chaotic behaviour, by a rising driving frequency f and a fixed driving amplitude $V = 0.28$. (B) The first Lyapunov exponent λ, for the same parameters of (A). $V_{C1} = -1.5$.

Figure 10: (A) A quasiperiodic torus T^2 for $f = 0.16600$. (B) The four-sided quasiperiodic folded torus for the critical parameter $f = 0.16899$. (C) The destruction of the torus leading to a type-II intermittency. (D) A chaotic attractor with a heteroclinic saddle disconnection for $f = 0.17000$. $V_{C1} = -1.5$.

For increasing f and a fixed V we see, in Fig. 10, a sequence of four figures showing the attractor modification on the Poincaré section at $V_{C1} = -1.5$.

The two-frequency torus (T^2) is created after a supercritical Hopf bifurcation. In this situation, before the onset of chaos, the torus is a deformed circle with no folds or cuspides, as shown in Fig. 10A ($f = 0.16600$). However, increasing the frequency to $f = 0.16899$, the torus T^2 grows in size and folds in four parts resembling a four-sided polygon (Fig. 10B). The torus breaks as in Fig. 10C ($f = 0.16900$) leading to the appearance of type-II intermittency [21], which causes the trajectory to evolve spirally around the previously existing repellor focus point, localized close to the origin of the angular frame in Fig. 10B. Increasing further the frequency we can hardly recognize the previous existing torus 10D.

In Fig. 10B the four folds of the T^2 torus can be recognized by the numbers 1,2,3, and 4. These folds are approaching four invisible saddle points (whose position could be determined by introducing noise); each pair of saddle points represents a period-two basic cycle. So, in the vicinity of the fold 4, there is an invisible basic cycle that crosses the section again near the fold
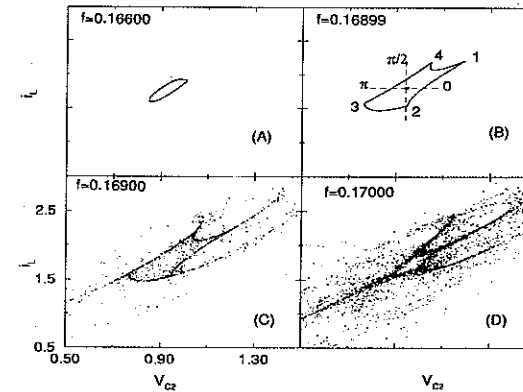
2. And the same occurs to the others folds, the cycle crosses from the fold 3 to the fold 1. Along the torus, not yet destroyed, a quasi-periodic trajectory is clockwise oriented with a winding number ($w = 0.4806\ldots$) near to the rational fraction $w = \frac{12}{25}$. Twelve is the number of the trajectory rotations along the torus to return back near the same point, taking twenty five complete poloidal cycles.

In Fig. 10C, after passing nearby each saddle point, the trajectory crosses this Poincaré section two times before returning to the same saddle point. We can consider the flow on this section as a mapping G. So, if c_n with $n = 1, \ldots, 4$, are the saddle points, then $G^2(c_n) = c_n$, $G(c_4) = c_2$, and $G(c_3) = c_1$.

As a matter of fact, the laminar spiral trajectory is a four-spiral trajectory, which means that the trajectory visits each time one of the four spirals. These spirals evolve approaching asymptotically the saddle points (Fig. 10C). In fact, each spiral tends to one of the four corners of the polygon. These corners, indicated by numbers, reach the saddle points when chaos shows up. These saddle points have two different unstable manifolds. Along one
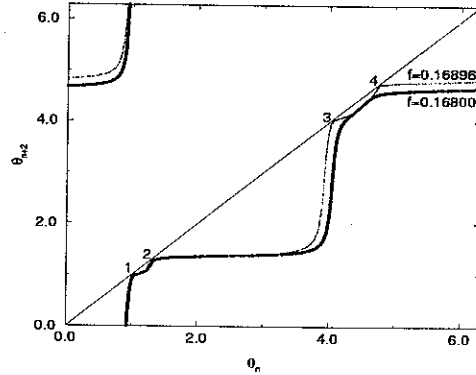
13

14

Figure 11: Angular period-two return map for two values of the parameter f indicated in figure. An evidence that, increasing f, the torus grows in size approaching two period-two saddle points.

unstable manifold of the saddle point the trajectory is ejected outside the polygon causing a chaotic burst, characteristic of intermittent regimes [21]. Along the other unstable manifold the trajectory is directed to the nearest saddle point in the clockwise direction, i.e., $G^2(c_4 + \epsilon)$ leaves c_4 to c_1, for example.

The angular frame shown in Fig. 10B is used to locate the four folds in an angular space. So, in Fig. 11 the angular period-two return map shows that before the torus breaks ($f = 0.16800$) there is no angular two period-two fixed points as shown by the large black line (although the large line seems to touch the identity straight line, it does not.). However, just before the torus breaks ($f = 0.16896$) we see that two period-2 fixed points will be formed by an infinitesimal increase of the parameter f.

Figure 12 shows a sketch of the flow of the mapping G^2. We see in (A) the stable two-frequency torus and the surrounding invisible four saddle points. Then, the torus grows in size, folding and touching the four saddle points. After the torus touches these points (B), it is no longer closed (since its breakdown already occured); the saddle points become visible, and form a heteroclinic saddle connection [25]. This heteroclinic saddle connection is the
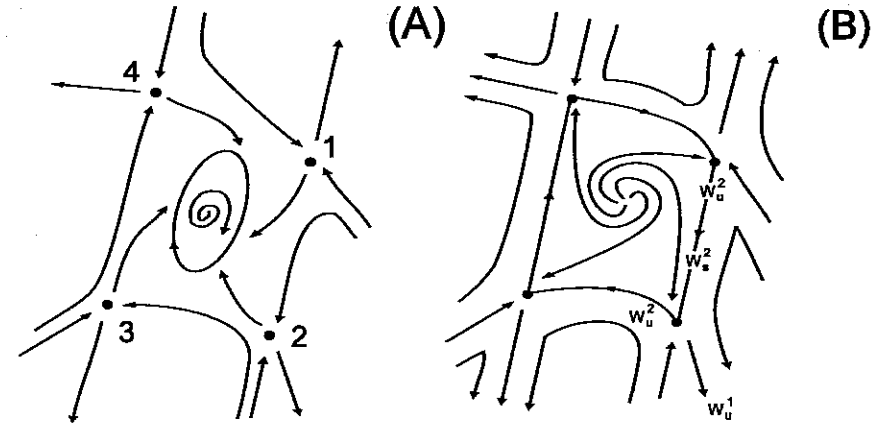

Figure 12: The geometry behind the torus breakdown. In this figure we see the flow of the mapping G^2 for the stable two-frequency torus (A) and for its breakdown forming the heteroclinic saddle connection (B).

nonlinear mechanism responsible for the chaotic burst and reinjection around the repellor focus, characteristics of type-II intermittent behavior [21].

After the heteroclinic saddle connection be created, increasing further the frequency generates the heteroclinic saddle disconnection where there is no longer the spiralling laminar behavior of the trajectory around the repellor focus. In fact, each one of the four-spirals turn into four-straight lines. It means that, after the trajectory be reinjected around the repellor focus, it approaches the saddle points along an oriented straight line, no more spiraling.

The unstable manifolds responsible for the chaotic burst are indicated in Fig. 12B by W_u^1, and by W_u^2 those responsible for the heteroclinic saddle connection (an orbit in G^2 that connects the two period-two saddle points). So, the unstable manifold of the saddle point 1 (indicated in Fig. 12A), $W_u^2(1)$ is the stable manifold of the point 3 (indicated in Fig. 11B) , $W_s^2(3)$. This heteroclinic loop is also called a Poincaré homoclinic contour [27].

In Fig. 13 we see a sequency of power spectra for a limit cycle (A) with frequency f, that suffers a Hopf bifurcation with the appearance of a second frequency f_2, originating a quasiperiodic two-frequency tori (B,C,D) only
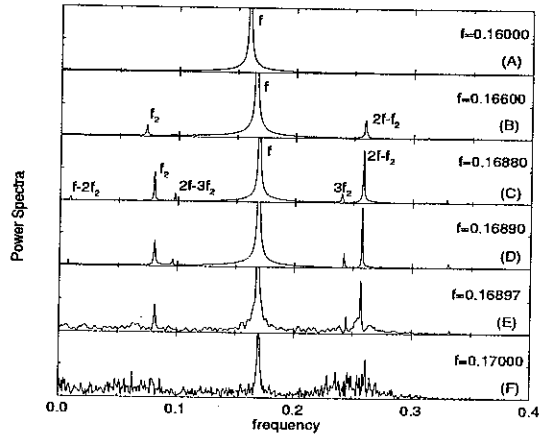
Figure 13: Sequence of power spectra, indicating phase-locking (A), quasi-periodic two-frequency tori (B,C,D), onset of chaos (E), and large chaotic band (F).

with frequencies $nf + mf_2$ $(n, m \; \epsilon N)$. Furthermore, in (E) we see the onset of chaos and in (F) a large chaotic band. So, we see in these spectra that for a very small change in the driving parameter a large chaotic band appears, what is different from the soft onset of chaos for which a large parameter variation is required to these chaotic bands become remarkable.

V. Conclusions

We analysed numerically the oscillations and the onset of chaos induced in the sinusoidally driven Double Scroll circuit. For varying driven parameters, the attractors were identified by power spectrum analyses, and by computing bifurcation diagrams and the first Lyapunov exponent. Furthermore, we described also topological changes due to the onset of chaos through two-frequency torus breakdown.

We showed that in the driven Double Scroll circuit chaos can appears directly through the breakdown of a two-frequency torus, when varying a parameter. Furthermore, we identified three possible scenarios for this transition: two in the Curry-Yorke route, and one through type-II intermittency.

Firstly, we found that, for the system considered in this work, the torus can softly breakdown to chaos through the route of Curry-Yorke [11]. One scenario for this route is when phase-locked trajectories become unstable and heteroclinic chaos shows up, as generally proposed in Ref. [13]. Moreover, in this case we identified the geometry (a transversal crossing to the strong stable foliation with the stable manifold of the knot) in the vicinity of the heteroclinic point (in the phase-locked trajectory that losed its stability). This is difficult to realize for a dissipative system like the driven Double Scroll circuit. Secondly, another identified scenario for the onset of chaos in the Curry-Yorke route is is the period-doubling bifurcations, like for instance, for the driven $p - n$ junction passive resonators circuit [15].

Furthermore, we recently identified another scenario for the onset of chaos in the analysed circuit [21], namely, the abrupt appearance of chaos through type-II intermittency. In this scenario, a two-frequency quasiperiodic torus looses its stability by touching the saddle points and forming a heteroclinic saddle connection. We identified this as the nonlinear mechanism responsible for the reinjection of the trajectory, around the repelor focus, that produces the laminar phase of the type-II intermittence.

These identified two-frequency torus breakdown to chaos, for a varying parameter, have two distinct dynamic characteristics. Chaos appears softly in the Curry-Yorke route, through phase-locking and period-doubling scenarios, and after chaos onset phase-locking is again observed. On the other hand, via type-II intermittence, chaos appears abruptlly and is preserved for a large range of the varying parameter.

Furthermore, the two-frequency torus breakdown preceeded by a torus-doubling, as reported in Refs. [28] and [29], was not seen for the considered system.

Generally, the Curry-Yorke route has another possible scenario for the onset of chaos through quasiperiodic two-frequency torus breakdown [14], not yet observed in the driven Double Scroll circuit. However, this scenario is difficult to observe since the attractors usually phase-lock before breaking. This happens because one must apropriately choose two parameter variations to mantain the attractor with the same irrational rotation (consequently, avoiding phase-locking).

Although, in this paper we only presented results for driving varying frequencies and fixed amplitudes, the vice-versa was also explored and lead to the same kind of conclusions.

Finally, the scenarios reported in this paper might be usefull to determine other scenarios for torus breakdown observed in other systems with two or more basic frequencies [30].

Acknowledgments

References

[1] E. Ott, *Chaos in dynamical systems*, Cambridge University Press, Cambridge (1993).

[2] K. T. Alligood, T. D. Sauer, J. A. Yorke, *Chaos, an introduction to dynamical systems*, Springer, New York (1997).

[3] M. L. Feigenbaum, J. Stat. Phys. **19**, 25 (1978).

[4] A. Libchaber, C. Laroche, and S. Fauve, J. Phys. Lett., **43**, L211 (1982).

[5] D. Ruelle and F. Takens, Commun. Math. Phys. **20**, 167 (1971).

[6] J. P. Gollup and H. L. Swinney, Phys. Rev. Lett. **35**, 927 (1975).

[7] H. L. Swinney and J. P. Gollub, Phys. Today **31**, 41 (1978).

[8] P. S. Linsay and A. W. Cumming, Physica D **40**, 196 (1989).

[9] C. Grebogi, E. Ott, and J. A. Yorke, Physica D **15**, 354 (1984).

[10] P. M. Battelino, Phys. Rev. A *38*, 1495 (1988).

[11] J. H. Curry and J. A. Yorke, Lect. Notes Math. **688**, 48 (1978).

[12] P. Bergé, *Le Chaos: théorie et experiences*. Eyrolles, Paris, 1988.

[13] D. G. Aronson, M. A. Chory, G. R. Hall, and R. P. McGehee, *Commun. Math. Phys.* **83**, 303-354 (1982).

[14] S. Ostlund, D. Rand, J. Sethna, and E. Siggia, *Physica D* **8**, 303-342 (1983).

[15] R. V. Buskirk and C. Jeffries, *Phys. Rev. A* **31**, 3332-3357, (1985).

[16] T. Matsumoto and L. O. Chua, IEEE Trans. Circuits Syst. **CAS-32**, 797 (1985).

[17] M. Itoh, H. Murakami, and L. O. Chua, Int. J. Bifurcation and Chaos **4**, 1721 (1994).

[18] K. Murali and M. Lakshmanan, Int. J. Bifurcation and Chaos **2**, 621 (1992).

[19] L. Pivka, A. L. Zheleznyak, and L. O. Chua, Int. J. Bifurcation and Chaos **4**, 1743 (1994).

[20] K. Murali and M. Lakshmanan, Int. J. Bifurcation and Chaos **1**, 369 (1991).

[21] M. S. Baptista and I. L. Caldas, submitted for publication.

[22] M. S. Baptista, "Perturbing non-linear systems, an overview for controlling chaos," Ph. D. thesis, University of São Paulo, São Paulo, IFUSP (1996).

[23] M. S. Baptista and I. L. Caldas, submitted for publication.

[24] S. Hayes, C. Grebogi, and E. Ott, *Phys. Rev. Lett.* **70**, 3031-3034 (1993).

[25] D. K. Arrowsmith and C. M. Place, *An Introduction to Dynamical Systems*, Cambridge University Press, UK, 1990.

[26] J. P. Eckmann and D. Ruelle, *Rev. Mod. Phys.* **57**, 617-656 (1985).

[27] L. P. Shil'nikov, Int. J. Bifurcation and Chaos **4**, 489 (1994).

[28] H. Tominaga and H. Mori, *Prog. Theor. Phys.* **91**, 1081-1099 (1994).

[29] J. Simonet, E. Brun, and R. Badii, *Phys. Rev. E* **52**, 2294-2301 (1995).

[30] V. S. Anishchenko, M. A. Safonova, U. Feudel, and J. Kurths, *Int. J. of Bifurcation and Chaos* **4**, 595-607 (1994).